ROYAL SOCIETY OF CHEMISTRY

PAPER

CrossMark
click for updates

Quantum-chemical study of stable, meta-stable and high-pressure alumina polymorphs and aluminum hydroxides†

Michael F. Peintinger,*[a] Michael J. Kratz[b] and Thomas Bredow[b]

The structure, electronic properties and relative stability of seven thermodynamically stable, meta-stable and high-pressure alumina polymorphs as well as the structure and relative stability of four aluminum hydroxides were calculated with periodic hybrid density functional theory calculations and compared with available experimental data. For a number of polymorphs several structure models that are discussed in the literature were compared in terms of their agreement with structural data and stability. In order to compare oxides and hydroxides the energies and heats of atomization of the latter were corrected by the reaction energy with water. The following overall energetic order was obtained: gibbsite < bayerite < boehmite < akdalaite < α-Al$_2$O$_3$ < κ-Al$_2$O$_3$ < θ-Al$_2$O$_3$ < δ-Al$_2$O$_3$ < γ-Al$_2$O$_3$ < η-Al$_2$O$_3$ < ι-Al$_2$O$_3$.

1. Introduction

Alumina (Al$_2$O$_3$) is one of the most important ceramic materials for technological applications. Corundum (α-Al$_2$O$_3$) is used in spark plugs due to its high electrical resistance, in parts of acid and brine pumps due to its corrosion resistance, in melting pots and thermocouple tubes due to its high temperature resistance and in prostheses because of its bio-compatibility. Also under high pressure conditions there are numerous technological applications for aluminum oxide. For example ruby (Al$_2$O$_3$ doted with Cr$_3$$^+$) is used as a pressure calibrator in "diamond-anvil-cells"[1] and sapphire (Al$_2$O$_3$ doted with various cations) as a window material in shock wave experiments.[2] Besides the thermodynamically stable corundum there is a variety of metastable alumina phases of technological importance.

The κ-modification is used for surface coating of cutting tools because of its extreme hardness.[3,4] Since the γ-phase provides a large surface due to its porous structure[5] it is used in as support and structural promoter in catalysts in synthesis,[6] for the reduction of automotive pollutants, oil refining and in absorbents.[7,8]

But alumina is also of high interest in recent fundamental material chemistry research. The properties of iron and titanium defects and aggregates in sapphire were theoretically investigated by Walsh and coworkers.[9] Bai and others have observed an improvement in the growth and dielectric properties of carbon nanotubes by hybridization with ceramic microparticles.[10] Carreon *et al.* have reported the synthesis of continuous cobalt–adeninate metal–organic framework (MOF) membranes supported on porous alumina tubes.[11] Very recently the synthesis and detailed structural studies of mesoporous alumina as thin films and as powders[12] were reported by Rønning *et al.* In energy research it was used as coating material for high voltage cathodes for enhanced electrochemical performance.[13] Alumina was even used in photochemistry to create and stabilize aqueous solutions of electrons[14] and the fabrication of free-standing Al$_2$O$_3$ nanosheets promise high mobility flexible graphene field effect transistors.[15]

Despite its technological importance, there was no comprehensive experimental or theoretical work that covered all known alumina phases. With this manuscript we now present the first extensive quantum-chemical investigation of the geometric and electronic structure and the relative stability for all known Al$_2$O$_3$ modifications.

Aluminium hydroxides, a family of the seven compounds akdalaite (tohdite),[16] bayerite,[17] boehmite,[18] diaspore,[19] doyleite,[20] gibbsite[17] and nordstrandite[20] were extensively studied by Demichelis *et al.* They recently published a complete, systematic, and homogeneous review investigating the physico-chemical properties at hybrid density functional theory level[21] employing the B3LYP functional. To investigate the role of electron correlation in the stability of the hydroxides, Casassa and Demichelis reinvestigated their findings with periodic local Møller–Plesset second-order perturbative approach, aiming at providing a reliable trend of stability on the basis of a proper description of both the long-range Coulomb interactions and the short-range correlation effects.[22]

[a]*Max Planck Institute for Chemical Energy Conversion, Stiftstrasse 34 - 36, 45470 Mülheim an der Ruhr, Germany. E-mail: michael.peintinger@gmail.com*

[b]*Mulliken Center for Theoretical Chemistry, Institut für Physikalische und Theoretische Chemie, University of Bonn, Beringstr. 4-6, D-53115 Bonn, Germany*

This journal is © The Royal Society of Chemistry 2014

J. Mater. Chem. A, 2014, **2**, 13143–13158 | **13143**

For comparison purposes we also include the four aluminum hydroxides boehmite (γ-AlO(OH)), gibbsite (γ-Al(OH)$_3$), bayerite (α-Al(OH)$_3$) and akdalaite (Al$_{10}$O$_{15}$·H$_2$O) in our study. The latter represent precursors of alumina phases which are formed during the calcination process.

Some phases are produced from other precursors, for example δ-Al$_2$O$_3$, which is also formed during thermal oxidation of aluminum.[23] The most common processing routes are shown in Fig. 1.

Boehmite represents the main component of many bauxite minerals and can be synthesized by precipitation of certain aluminum salts in aqueous solution or by hydrothermal synthesis just as gibbsite and bayerite.[24] Gibbsite is also a part of bauxite minerals[25] whereas the structurally related bayerite is rarely found in nature.[23] In addition to the above-mentioned ways it can be produced with the Bayer process.[23] Akdalaite is most commonly processed from gibbsite by hydrothermal synthesis.[26]

In the metastable polymorphs, the oxygen anions form either face-centered cubic (fcc) or hexagonal close-packed (hcp) lattices.[23] The distribution of cations within these lattices results in a large number of different polymorphs. The structures based on the fcc packing of the oxygen atoms include γ, η (cubic), θ (monoclinic), δ (either tetragonal or orthorhombic) and γ' (tetragonal). The structures based on the hcp packing include α (trigonal), κ (orthorhombic), κ' (hexagonal) and ι (orthorhombic). Additional phases named θ', θ'', λ (all monoclinic), U (orthorhombic) and χ (cubic[27] or hexagonal[28]) have been mentioned in the literature but were discarded in the present study because the reported structure data are incomplete. U–Al$_2$O$_3$ was discovered in nanocomposite Al$_2$O$_3$–SiC coatings using XRD.[29] θ'–, θ''–, λ-Al$_2$O$_3$ were found by Levin *et al. via* electron diffractometry and high-resolution electron microscopy in plasma-sprayed Al$_2$O$_3$ layers and in amorphous, anodic Al$_2$O$_3$ films.[30–32] χ-Al$_2$O$_3$ is formed during calcination of gibbsite and represents the structural transition from gibbsite to κ-Al$_2$O$_3$.[23] It is assumed that the χ phase has a complex layer structure with a random stacking order where the oxygen atoms are similarly packed as in gibbsite.[28]

Moreover, we investigate several existing structural models of high-pressure alumina phases. It is known that corundum is transformed into the so-called Rh$_2$O$_3$ phase at about 80–100 GPa which turns into the CaIrO$_3$ phase at about 130 GPa. In order to overcome the kinetic barriers between these modifications, temperatures above 1000 °C are needed.[33,34] As there are to our knowledge no recent extensive studies of the structure and properties of these high-pressure phases, the results of the present theoretical study may be useful for future studies, *e.g.* on phase transformations, surface and adsorption studies as well as reaction paths.

Details of our computational approach can be found in the section Computational details.

2. Results and discussion

2.1 Aluminum hydroxides

The calculated lattice constants are given in Tables 1–4. They show good agreement with experimental values with relative errors of less than 0.9% for boehmite, 2.8% for gibbsite, 0.8% for bayerite, and 0.6% for akdalaite, respectively.

It should be mentioned that the layer structures may be slightly improved with an additional dispersion correction to DFT.[35] In this study no dispersion correction was applied because the effects are expected to be small.

In order to include the hydroxides to the comparison of the relative stability of the alumina phases where the atomization enthalpy $\Delta_A H^0$ was taken as measure, the atomization enthalpy $\Delta_A^* H^0$ of Al$_2$O$_3$ was recalculated from the reaction enthalpy $\Delta_R H^0$ of the hydroxides and H$_2$O and normalized to one formula unit Al$_2$O$_3$.

$$\Delta_A^* H^0_{Al_2O_3} = \Delta_R H^0_{Al_2O_3} + 2H^0_{Al} + 3H^0_O \tag{1}$$

Table 1 Boehmite bulk properties, lattice constants a, b, c (Å) and adjusted heat of atomization $\Delta_A^* H^0$ (kJ mol^{-1})

	Calc.	Exp.[a]
a	2.872	2.876
b	12.125	12.24
c	3.742	3.709
$\Delta_A^* H^0$	3090	—

[a] Ref. 36.

γ-AlO(OH) (Boehmite) $\xrightarrow{300°-500°C}$ γ- $\xrightarrow{700°-800°C}$ δ- $\xrightarrow{900°-1000°C}$ θ- $\xrightarrow{1000°-1100°C}$ α-Al$_2$O$_3$

γ-Al(OH)$_3$ (Gibbsite) $\xrightarrow{150°-300°C}$ χ- $\xrightarrow{650°-750°C}$ κ- $\xrightarrow{1000°C}$ α-Al$_2$O$_3$

α-Al(OH)$_3$ (Bayerite) $\xrightarrow{200°-300°C}$ η- $\xrightarrow{600°-800°C}$ θ- $\xrightarrow{1000°-1100°C}$ α-Al$_2$O$_3$

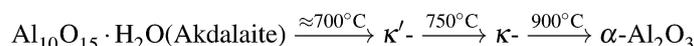Al$_{10}$O$_{15}$·H$_2$O(Akdalaite) $\xrightarrow{\approx 700°C}$ κ'- $\xrightarrow{750°C}$ κ- $\xrightarrow{900°C}$ α-Al$_2$O$_3$
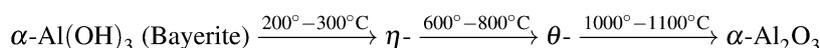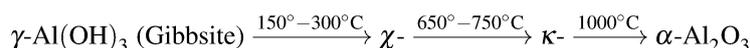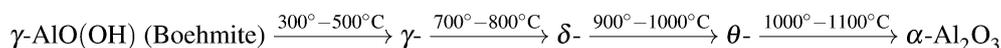
Fig. 1 Common calcination routes of aluminum hydroxides and phase transitions of metastable aluminum polymorphs towards the formation of corundum.[23]

Table 2 Gibbsite bulk properties, lattice constants a, b, c (Å), β (degrees) and adjusted heat of atomization $\Delta_A^* H^0$ (kJ mol^{-1})

	Calc.	Exp.[a] SG $P2_1/c$
a	9.681	9.736
b	5.064	5.078
c	12.877	12.523
β	137.8	136.3
$\Delta_A^* H^0$	3194	—

[a] Ref. 37.

Table 3 Bayerite bulk properties, lattice constants a, b, c (Å), β (degrees) and adjusted heat of atomization $\Delta_A^* H^0$ (kJ mol^{-1})

	Calc.	Exp.[a] SG $P2_1/c$
a	9.348	9.425
b	8.699	8.672
c	10.610	10.679
β	151.5	151.7
$\Delta_A^* H^0$	3185	—

[a] Ref. 38.

Table 4 Akdalaite bulk properties, lattice constants a, c (Å), and adjusted heat of atomization $\Delta_A^* H^0$ (kJ mol^{-1})

	Calc.	Exp.[a]
a	5.612	5.576
c	8.777	8.768
$\Delta_A^* H^0$	3014	—

[a] Ref. 39.

The enthalpies H^0 have been calculated including zero point energies and vibration contributions at 298 K. The atomic energies were corrected from basis set superposition error with the counterpoise method (ATOMBSSE).

$$\text{Boehmite}: \ \Delta_R H^0_{Al_2O_3} = 2H^0_{AlO(OH)} - H^0_{H_2O} \qquad (2)$$

$$\text{Gibbsite and Bayerite}: \ \Delta_R H^0_{Al_2O_3} = 2H^0_{Al(OH)_3} - 3H^0_{H_2O} \qquad (3)$$

$$\text{Akdalaite}: \ \Delta_R H^0_{Al_2O_3} = 1/5\left(H^0_{Al_{10}O_{15}\cdot H_2O} - H^0_{H_2O}\right) \qquad (4)$$

2.1.1 Boehmite – γ-AlO(OH). The aluminum and oxygen atoms form double layers of octahedra between which the hydrogen atoms are located in a zig-zag fashion (Fig. 2). The exact position of the hydrogens and therefore the space group is not fully known. In a previous study Digne et al.[40] suggest that at room temperature, the space group $Cmcm$ is most probable boehmite. Therefore we take the orthorhombic model (space group $Cmcm$, no. 63) proposed by Christensen et al.[36] from neutron powder diffraction as a starting structure for our geometry optimizations.

2.1.2 Gibbsite – γ-Al(OH)₃. Saalfeld and Wedde[37] investigated the gibbsite structure with XRD and suggested that it
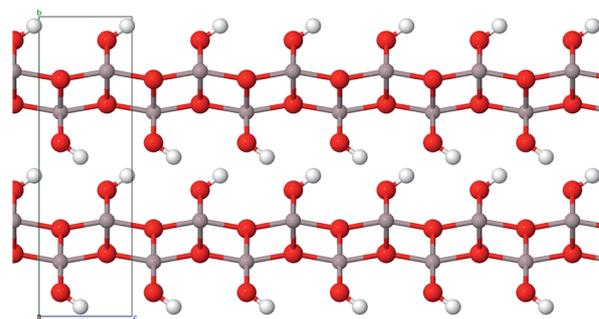

Fig. 2   Layer structure of boehmite (color code: Al grey, O red, H white).

consists of layers of AlO₆-octahedra that share one edge along the plane whereby each oxygen atom is bonded to one hydrogen atom. Half of the hydrogen atoms form hydrogen bridges within the layers whereas the other half forms inter-layer bridges (Fig. 3). The suggested monoclinic primitive unit cell contains eight formula units (space group $P2_1/n$). As $P2_1/n$ is a non-standard space group, the atomic positions and lattice constants were transformed to the standardized space group $P2_1/c$ (no. 14) for the CRYSTAL calculations. For the applied transformation matrices see ref. 41.

2.1.3 Bayerite – α-Al(OH)₃. The structure of bayerite is very similar to the structure of gibbsite regarding the layers. The main difference is the arrangement of the hydrogen bonds between the layers (see Fig. 3 and 4).[40] Zigan et al.[38] have suggested a primitive unit cell containing eight formula units with the space group $p2_1/n$ based on XRPD results. As discussed above for gibbsite, the atomic positions and lattice constants were transformed to the standard setting in space group $P2_1/c$.

2.1.4 Akdalaite – Al₁₀O₁₅·H₂O. Yamaguchi et al. have used XRD and a least-squares refinement to determine the atomic positions of the hydrogen and oxygen atoms and the space group ($p6_3mc$, no. 186).[39] The oxygen atoms (positions 2b, 2a and 6c) form close-packed layers that are stacked in an ABAC fashion. Within the hexagonal primitive unit cell eight aluminum atoms build slightly distorted AlO₆-octahedra (position 6c and 2b) whereas the remaining two (position 2b) form also slightly distorted AlO₄-tetrahedra (Fig. 5). Digne et al.[40] obtained a structure where the hydrogen atoms occupy the
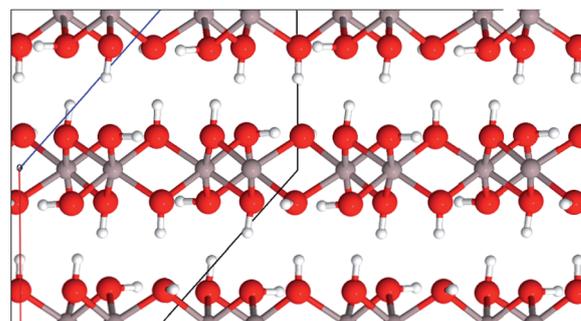

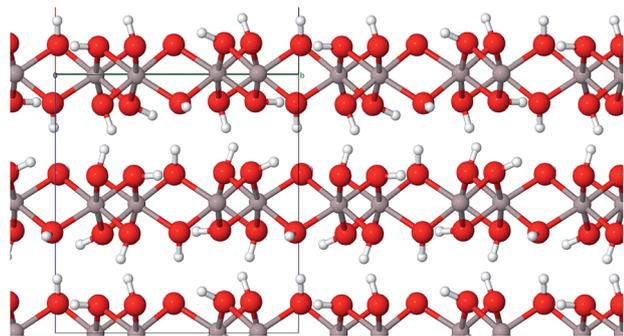Fig. 3   Layer structure of gibbsite (color code: Al grey, O red, H white).

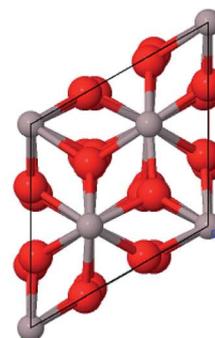Fig. 4 Layer structure of bayerite (color code: Al grey, O red, H white).

position 2a $(0, 0, z)$. Therefore we put the hydrogen atoms in the same position with a z-value of 0.125 which results in an initial O–H distance of about one Angstrom.
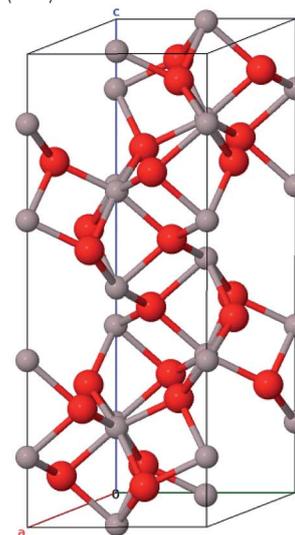
2.2 Alumina phases

2.2.1 α-Al₂O₃. α-Al$_2$O$_3$ crystallizes in the trigonal crystal system (space group R$\bar{3}$c, no. 167) and can be described with either a rhombohedral or a hexagonal lattice system. The oxygen atoms form an hcp packing of spheres where 2/3 of the octahedral vacancies are occupied by aluminum atoms. The conventional unit cell (hexagonal axes, see Fig. 6) contains 30 atoms (Al$_{12}$O$_{18}$, primitive cell: Al$_4$O$_6$) where the oxygen atoms occupy position 18e $(x, 0, 0.25)$ and the aluminum atoms occupy position 12c $(0, 0, z)$.[23] Different from the ideal hcp cell the values of the x- and z-coordinate ($x = 0.307$ and $z = 0.352$)[42] differ from the value 1/3 because the aluminum atoms move towards the unoccupied octahedral interstices and hereby induce a repositioning of the oxygen atoms as well.[23]

The calculated bulk properties are shown in Table 5. After relaxation the atomic positions are almost identical to the experimental data and the results for the lattice constants are very satisfying as well with a relative error of 0.8%. The calculated heat of atomization $\Delta_A H^0$ of 3005 kJ mol^{-1} (corrected by the basis set superposition error (BSSE)) is 78 kJ mol^{-1} below the experimental value and thus shows an acceptable error of 2.5%. A study with electron energy loss spectroscopy (EELS)[44] yielded a fundamental band gap of 8.5 eV that is very close to the calculated 8.6 eV. The band

(a) View along $\langle 001 \rangle$

(b) Perspective

Fig. 6 Conventional hexagonal unit cell of α-Al$_2$O$_3$.

structure yields a HOCO–LUCO-transition at the Γ-point (HOCO, highest occupied crystalline orbital; LUCO, lowest unoccupied crystalline orbital) which is consistent with a previous theoretical study.[45] From the projected density of states (PDOS) it can be concluded that the valence band consists mainly of oxygen orbitals and the conduction band mainly of aluminum orbitals as it is expected for an ionic compound in the form of Al$_2^{3+}$O$_3^{2-}$. Band structures, atomic positions and density of states for all investigated modifications are listed in the ESI.†

Fig. 5 Structure of akdalaite, view along $\langle 010 \rangle$ (color code: Al grey, O red, H white).

Table 5 α-Al$_2$O$_3$ bulk properties, lattice constants a, c (Å), heat of atomization $\Delta_A H^0$ (kJ mol^{-1}), fundamental band gap BG (eV) and atomic parameters x and z

	Calc.	Exp.[a]
A	4.788	4.761
C	13.032	12.996
$\Delta_A H^0$	3005	3083[b]
BG (direct)	8.6	8.5[c]
Z	0.019	0.019
X	−0.361	−0.360

[a] Ref. 42. [b] Ref. 43. [c] Ref. 44.

13146 | J. Mater. Chem. A, 2014, 2, 13143–13158

This journal is © The Royal Society of Chemistry 2014

2.2.2 κ-Al₂O₃. The κ modification has orthorhombic symmetry[46] and the space group $Pna2_1$ (no. 33).[47] Studies with HREM, XRPD, TEM (transmission electron microscopy) and NMR (nuclear magnetic resonance) led to structures where the aluminum atoms are octahedrally as well as tetrahedrally coordinated by oxygen atoms.[48,49] There are 40 atoms within the primitive unit cell ($Al_{16}O_{24}$) in which the oxygen atoms form ABAC layers where 3/4 of the aluminum atoms are situated in octahedral and 1/4 in tetrahedral interstices (see Fig. 7). Within the space group $Pna2_1$ there is only the position 4a (x, y, z) which is consequently occupied by all atoms. The structure found by Ollivier $et\ al.$[49] with XRPD is serving as the starting structure in this work.

With a relative error of less than 1% pob-DZVP/PW1PW provides good results for the lattice constants (Table 6). For the band gap a vertical transition of 7.4 eV was calculated in this work whereas a theoretical study on the electronic structure of four Al_2O_3 modifications by Lee $et\ al.$[51] predicted a band gap of 5.49 eV. In the same study the band gap of corundum was underestimated by 2 eV which can be addressed to the use of the LDA functional and the well-known self-interaction error.

2.2.3 θ-Al₂O₃. The conventional monoclinic unit cell (space group $C2/m$, no. 12) contains 20 atoms (Al_8O_{12}, prim. cell: Al_4O_6) that all occupy position 4i $(x, 0, z)$ (Fig. 8). The aluminum atoms are evenly distributed over the octahedral and tetrahedral interstices of the oxide lattice.[7] For the initial structure we used the data from an XRPD study of Husson and Repelin.[52]
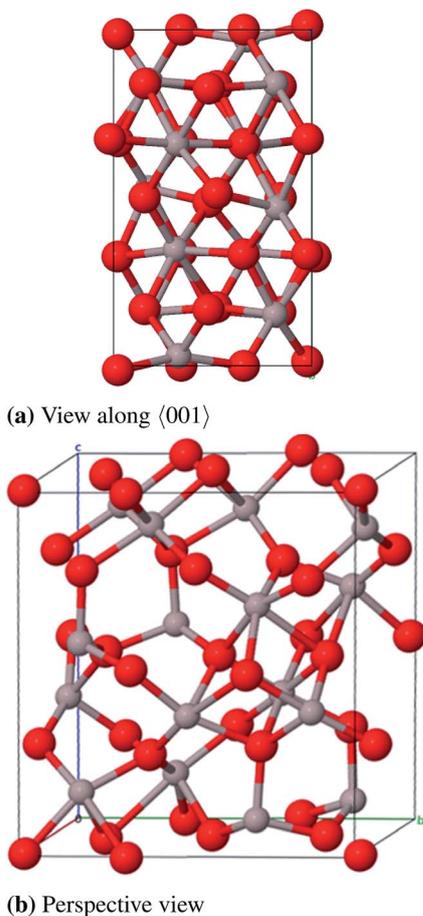
Table 6 κ-Al₂O₃ bulk properties, lattice constants a, b, c (Å), heat of atomization $\Delta_A H^0$ (kJ mol⁻¹) and fundamental band gap BG (eV)

	Calc.	Exp.[a]
a	4.870	4.844
b	8.355	8.330
c	8.968	8.955
$\Delta_A H^0$	2982	3068[b]
BG (direct)	7.4	—

[a] Ref. 49. [b] Ref. 50.

(a) View along ⟨001⟩

(b) Perspective view

Fig. 7 Primitive unit cell of κ-Al₂O₃.

(a) View along ⟨010⟩

(b) Perspective

Fig. 8 Conventional unit cell of θ-Al₂O₃.

This journal is © The Royal Society of Chemistry 2014

J. Mater. Chem. A, 2014, 2, 13143–13158 | 13147
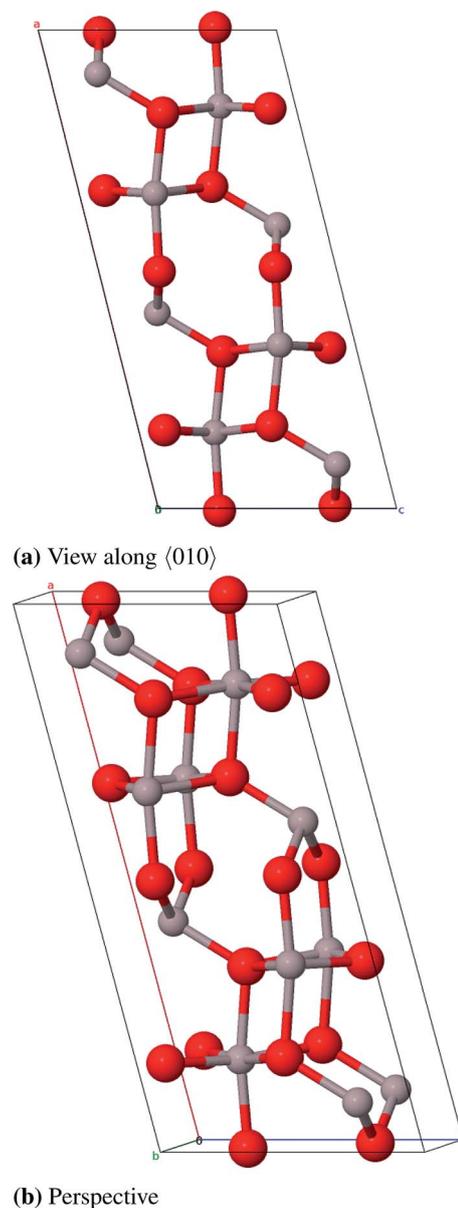
The calculated lattice constants are listed in Table 7 and agree well with experimental data presenting a relative error of 1.4%. An indirect band gap of 6.9 eV was calculated and may be compared to the value of 5.04 eV from Lee et al.[51] with an assumed underestimation of about 2 eV as discussed above.

2.2.4 γ-Al$_2$O$_3$. Because of the low crystallinity of this phase the exact determination of the structure is very complicated.[53] Ching et al.[54] even suggested that there is no long-range order at all to be found in γ-Al$_2$O$_3$. In many studies, primarily older ones, the structure is described as a defective cubic spinel type (space group $Fd\bar{3}m$, no. 227) that is composed of a close-packed oxygen lattice (position 32e) whose tetrahedral (position 8a) and octahedral interstices (position 16d) are occupied by aluminum atoms. As the anion–cation ratio is 4 : 3 in an ideal spinel, cation vacancies have to occur to ensure the correct stoichiometry of aluminum oxide (2 : 3).[55] Moreover a slight tetragonal distortion was reported in 1964 based on XRD results (0.983 < a/c < 0.987).[56] There have been a large number of experimental and theoretical studies to determine the octahedral–tetrahedral ratio in which the vacancies appear and to illuminate whether hydrogen is a part of the structure. It was concluded that hydrogen is only a part of the surface structure and thus does not appear within the bulk.[57,58] The vacancy ratio is a controversial issue as investigations with XRD, neutron powder diffraction and electron microscopy reveal that vacancies are located only in octahedral positions,[59,60] or only in tetrahedral positions[61,62] or in both octahedral and tetrahedral positions.[63] The latter result is also backed up by NMR and theoretical studies by Lee et al.[64] However, a variety of theoretical studies result in solely octahedral vacancies.[58,65–67] It has also been reported that several "non-spinel" positions are occupied in γ-Al$_2$O$_3$[68,69] and that the unit cell was tetragonal with $a_{cubic} = \sqrt{2}a_{tetragonal}$.[69] This tetragonal structure can be regarded as a contraction of the cubic lattice along one direction with the space group $I4_1/amd$ (no. 141) which is a maximum subgroup of $Fd\bar{3}m$.

Calculated diffraction patterns of cubic and tetragonal models where "non-spinel" positions are occupied have agreed very well with experimental data unlike diffraction patterns of defective spinel structure models.[53,70] Paglia et al. have created supercells (160 atoms) with the space group $Fd\bar{3}m$ as well as $I4_1/amd$ where aluminum atoms occupy "non-spinel" positions. This approach led to structures with the general space group $P1$

whose total energies were a little bit higher than the one of a defective spinel structure, but whose diffraction patterns correspond very well with experimental findings. Due to the poor crystallinity such a supercell can only be an approximation to the real structure of γ-Al$_2$O$_3$, but at the same time it contains all the representative characteristics of this phase. In general a random vacancy distribution is found in defective structures which is reflected only by a statistical mean value of many different defective cell models. As a consequence it is reasonable to choose the cell size as large as possible but as a consequence also the number of possible configurations and the computational costs increase along with the cell size.

Based on comparison of the diffraction patterns, Paglia et al.[69] concluded that γ-Al$_2$O$_3$ produced from boehmite can be better described with space group $I4_1/amd$ than with $Fd\bar{3}m$. It was noted that the experimental diffraction patterns can vary if different precursors are used. For example γ-Al$_2$O$_3$ produced from amorphous precursors via CVD could be better described by $Fd\bar{3}m$.

In this study we compare the structure model of Paglia et al. (space group $I4_1/amd$, no. 141) and the defective spinel model. A recent model for γ-Al$_2$O$_3$ by Menendez-Proupin and Gutierrez[53] was not included as it was developed by relaxing a defective spinel model without preserving the crystallographic system which we want to maintain for all structures.

But we want to mention that Ferreira et al. have compared this spinel-like structure proposed by Menendez-Proupin and Gutierrez[53,71] to a triclinic structure proposed by Pinto et al.[72] regarding their thermodynamic stability, lattice vibrational modes, and bulk electronic properties using DFT calculations.[73] They found the spinel-like model to be thermodynamically more stable by 4.55 kcal mol^{-1} per formula unit on average from 0 to 1000 K. Also the simulated infrared spectra of the spinel-like model showed better agreement with experimental data.

For the defective spinel model (γ-spinel) we started with a tripled primitive unit cell (Al$_6$O$_8$ → Al$_{18}$O$_{24}$) and removed two cations in octahedral positions in a way that the resulting vacancies are as far away from each other as possible. This stoichiometric cell contains 40 atoms (Al$_{16}$O$_{24}$) and is relaxed under the restriction that the cubic crystal system is maintained at all times (Fig. 9). All defective structures in this work were relaxed while maintaining the specific crystal system. For model (γ-P) of Paglia et al. we chose the most stable structure that they obtained by optimizing a $2 \times 1 \times 3$-$I4_1/amd$ supercell with frozen lattice parameters (Fig. 10).

Regarding the large number of atoms in the primitive cell (160) and the symmetry lowering due to the removal of individual atoms, the calculation of the γ-P-model is very expensive. Therefore no frequency calculation could be performed in this case. The lattice constants (Table 8 and 9) agree very well to the experimental data with relative errors of 0.2% (γ-spinel) and 0.9% (γ-Paglia). The calculated band gaps differ by about 1 eV from the experimental reference, but in contrast to the spinel-model a direct transition was calculated for the Paglia-model. Energetically the spinel-model lies 12 kJ mol^{-1} (per formula unit) below the Paglia-model and is closer to the experimentally

Table 7 θ-Al$_2$O$_3$ bulk properties, lattice constants a, b, c (Å), β (degrees), heat of atomization $\Delta_A H^0$ (kJ mol^{-1}) and fundamental band gap BG (eV)

	Calc.	Exp.[a]
a	11.803	11.795
b	2.932	2.910
c	5.650	5.621
β	103.9	103.79
$\Delta_A H^0$	2982	—
BG (indirect)	6.9	5.0[b]

[a] Ref. 52. [b] Ref. 51.

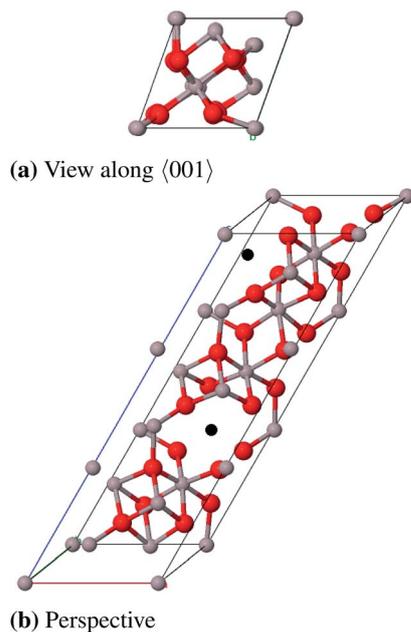**(a)** View along $\langle 001 \rangle$

(b) Perspective

Fig. 9 Primitive unit cell of γ-spinel-Al$_2$O$_3$ ($\alpha = \beta = \gamma = 60°$), vacancies are marked black.

found heat of atomization. This is in agreement with the findings of Ferreira *et al.* mentioned above.

However, in conclusion we favor the Paglia-model as representative bulk structure for γ-Al$_2$O$_3$ because (a) Paglia *et al.* showed that the diffraction patterns agree very well with experimentally found patterns and (b) the periodic defective spinel model would lead to a structure with a highly ordered distribution of vacancies. This feature is rather known for the thermodynamically more stable δ phase and would not fit the picture of a structure with a minor long-range order. Moreover, due to the enormous number of possible modifications Paglia *et al.* could not investigate all potential cells that can be derived from their approach, so it is likely that there exist energetically more favorable structures than the model we used.

2.2.5 η-Al$_2$O$_3$. In analogy to γ-, η-Al$_2$O$_3$ is a defective spinel structure (space group $Fd\bar{3}m$, no. 227) where several aluminum atoms occupy the 48f-position.

Shirasuka *et al.*[74] concluded from an XRPD study that 5/8 of the aluminum atoms are situated on the octahedral 16c- and 16d-position and the remaining 3/8 are distributed over the tetrahedral 8a- and 48f-positions. The results of a high-resolution transmission electron microscopy (HRTEM) study by Ernst *et al.*[75] differ from those of Shirasuka *et al.* only in the distribution of the cations over the 8a- (5.35%) and 48f-position (32.15%) while the 16c- and 16d-positions are occupied to the same amount.

Based on a Rietveld refinement Zhou and Snyder[68] suggested that the 8a- and 16c-positions are unoccupied and furthermore that about 10% of the aluminum atoms are situated on the "non-spinel" position 32e. But it is not yet clarified whether the latter model is only restricted to the surface region or not.
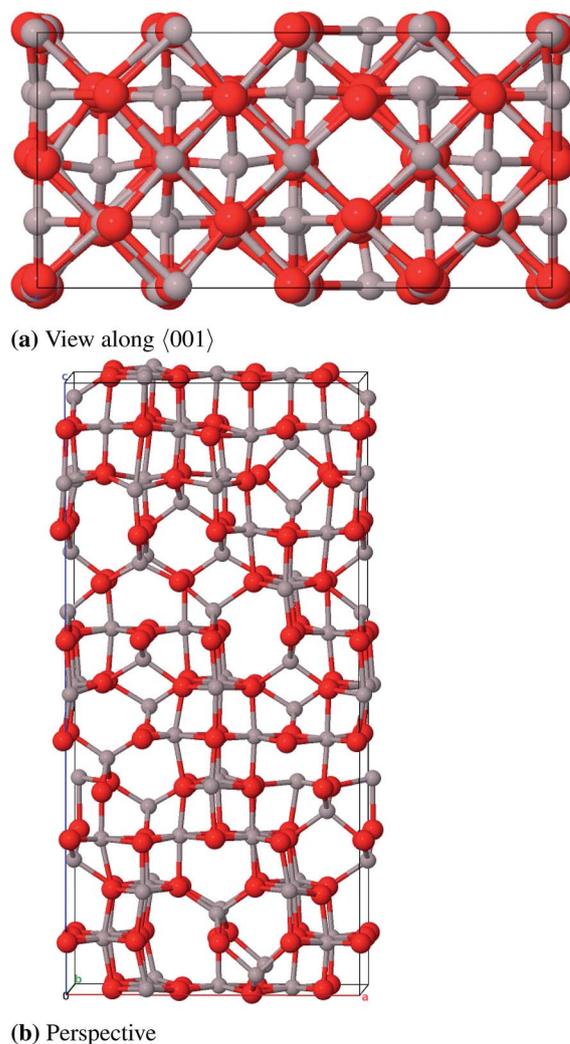

(a) View along $\langle 001 \rangle$

(b) Perspective

Fig. 10 Primitive unit cell of γ-P-Al$_2$O$_3$.

Table 8 γ-Spinel-Al$_2$O$_3$ bulk properties, lattice constant a (Å), heat of atomization $\Delta_A H^0$ (kJ mol^{-1}) and fundamental band gap BG (eV)

	Calc.	Exp.
a	7.930	7.911[a]
$\Delta_A H^0$	2966	3061[b]
BG (indirect)	6.2	—

[a] Ref. 68. [b] Ref. 50.

Table 9 γ-Paglia-Al$_2$O$_3$ bulk properties, lattice constants a, c (Å), heat of atomization $\Delta_A H^0$ (kJ mol^{-1}) and fundamental band gap BG (eV)

	Calc.	Exp.
A	5.661	5.616[a]
c	7.840	7.835[a]
$\Delta_A H^0$	—	3061[b]
BG (direct)	5.2	—

[a] Ref. 69. [b] Ref. 50.

Table 10 η-Al_2O_3 bulk properties, lattice constant a (Å), heat of atomization $\Delta_A H^0$ (kJ mol^{-1}) and fundamental band gap BG (eV)

	η-E Calc.	η-ZS Calc.	Exp.[a]
a	7.962	8.129	7.914
$\Delta_A H^0$	2930	2890	—
BG (indirect)	4.4	5.5	—

[a] Ref. 68.

It was reported by Lippens and De Boer[56] that there is a slight tetragonal distortion ($0.985 < a/c < 0.993$) and that the oxide lattice is less ordered than in γ-Al_2O_3.

In this study we employ Zhou and Snyders model (η-ZS) and the one proposed by Ernst (η-E). For both models we constructed two $1 \times 1 \times 3$-supercells leading to a composition of $Al_{72}O_{24}$ for η-ZS and $Al_{66}O_{24}$ for η-E assuming that all positions are fully occupied. Hence 56 and 50 atoms, respectively, had to be removed to achieve the correct stoichiometry. We removed the atoms in such a way that all the remaining interatomic distances are as large as possible. This procedure led to several structures for both models. The energetically most favorable version was selected as representative for the specific model.

We could not find a model of η-E where less than three atomic pairs exhibit a distance of 1.8 Å (Fig. 11a). After geometry optimization however those atoms lie at least 2.8 Å apart (Fig. 11b). For the η-ZS models we could only reduce the amount of 1.8 Å bonds to six (Fig. 12a) but in the relaxed structure the bonds are all $\geq$2.8 Å (Fig. 12b).

Fig. 12c and 11c show the distortion of the oxide lattice of η-ZS-Al_2O_3 compared to η-E-Al_2O_3. Regarding the relative errors of the calculated lattice constants (0.6% vs. 2.6%) and the heat of atomization (2930 kJ mol^{-1} vs. 2890 kJ mol^{-1}) we conclude that η-E-Al_2O_3 is the preferable model (Table 10). Moreover, as mentioned above, the Zhou and Snyder model may be restricted to the surface region. Both structures have indirect band gaps (4.4 eV and 5.5 eV) that are rather small compared to the other modifications.

2.2.6 δ-Al_2O_3. δ-Al_2O_3 was described by Wilson[76] and Lippens and De Boer[56] as a tripled cell of γ-Al_2O_3 with a highly ordered cation arrangement.[61] In previous studies a tetragonal ($a_\delta = b_\delta = a_\gamma$, $c_\delta = 3a_\gamma$)[56,77,78] and an orthorhombic unit cell was suggested ($a_\delta = a_\gamma$, $b_\delta = 1.5a_\gamma$, $c_\delta = 2a_\gamma$).[30,32,61] The tetragonal unit cell was found in those studies that produced δ-Al_2O_3 from boehmite, whereas orthorhombic symmetry was observed in studies that used other precursors. As there is not sufficient information available about the atomic positions of the orthorhombic cell we restricted ourselves to tetragonal δ-Al_2O_3.

Tsybulya and Kryukova[79] have obtained refined lattice constants through XRPD and electron microscopy and suggested the space group $P4_12_12$ (no. 92). The cation vacancies are distributed over octahedral positions.[76,78,80]

Coincidently γ-Fe_2O_3 is also composed of a tripled (spinel) cell with cation vacancies exclusively on octahedral positions and has the same space group $P4_12_12$,[81] therefore this model has already been used for calculations of δ-Al_2O_3.[82] Repelin and Husson[78] made a "least-squares fitting" of X-ray diffraction

(a) before relaxation

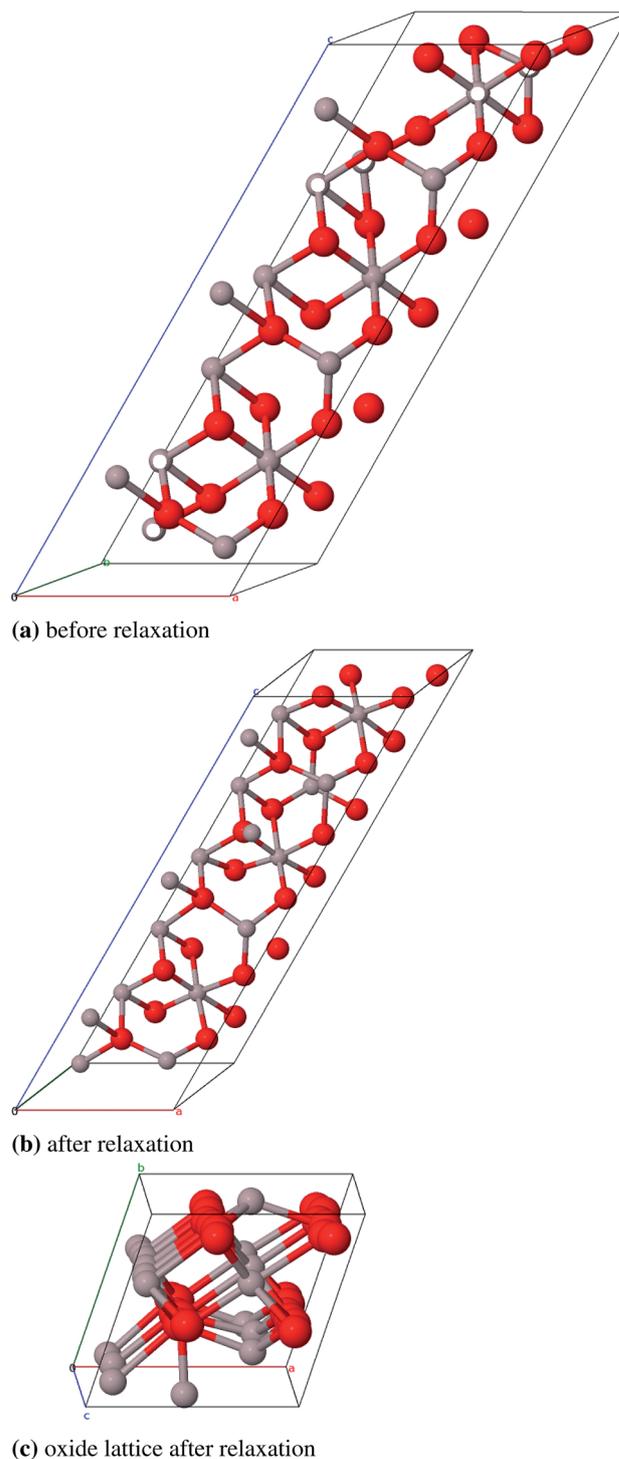**(b)** after relaxation

(c) oxide lattice after relaxation

Fig. 11 Primitive unit cell of η-E-Al_2O_3 ($\alpha = \beta = \gamma = 60°$), atom pairs with $d = 1.8$ Å are marked white, with d_{geq} 2.8 Å grey.

patterns of δ-Al_2O_3 which resulted in different lattice constants ($a_\delta \approx a_\gamma/\sqrt{2} = 5.599$ Å and $c_\delta = 23.657$ Å) that match well with a tripled cell of tetragonal γ-Al_2O_3.[69] In this work we have used the γ-Fe_2O_3-(δ-FE) as well as the Repelin–Husson-model (δ-RH, space group $P\bar{4}m2$, no. 115) as starting structures. It should be mentioned that Pecharroman et al.[83] concluded that the IR- and
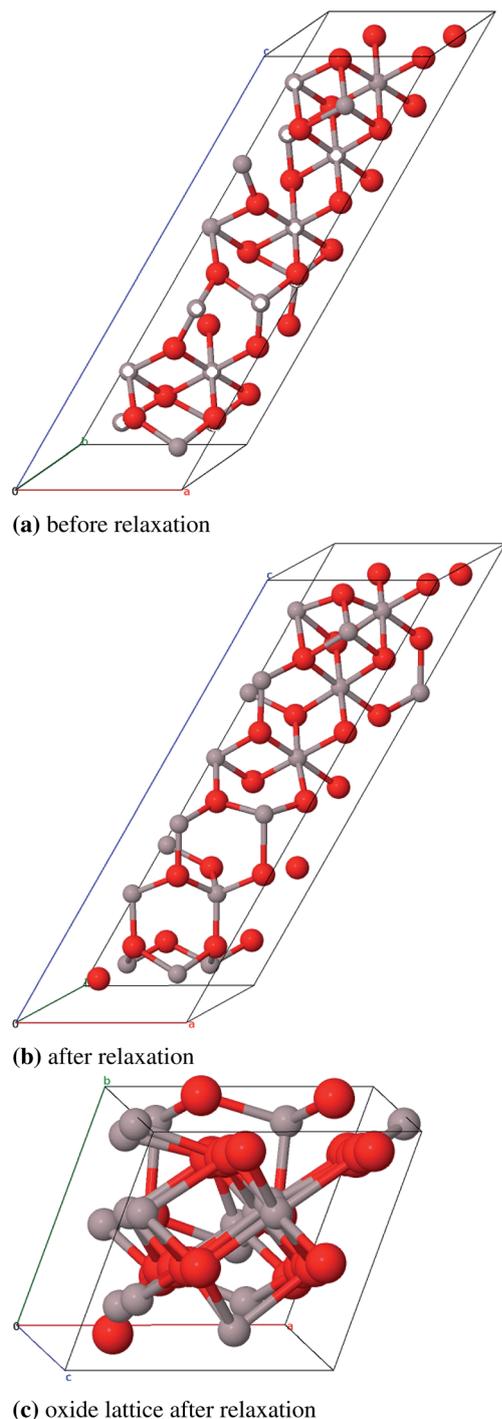
13150 | J. Mater. Chem. A, 2014, **2**, 13143–13158

This journal is © The Royal Society of Chemistry 2014

(a) before relaxation

(b) after relaxation

(c) oxide lattice after relaxation

Fig. 12 Primitive unit cell of η-ZS-Al_2O_3 ($\alpha = \beta = \gamma = 60°$), atom pairs with $d = 1.8$ Å are marked white, with d_{geq} 2.8 Å grey.

NMR spectra of δ-Al_2O_3 would rather fit to a mix of θ- and γ-Al_2O_3 than to a tripled spinel cell based on a spectra comparison of γ-Fe_2O_3 and δ-Al_2O_3.

We simplified the δ-RH model (80 atoms) concerning the actual occupancy of the six 4j (x, 0, z) and 4k (x, 1/2, z) positions of the aluminum atoms (each 83.3%) to be able to build a cell with less than 240 atoms: One 4j and 4k position is fully occupied while three of the remaining four positions are occupied.

Consequently there are four cation vacancies in this model which were positioned as far away from each other as possible (Fig. 13a). The crystallographic data for the δ-FE model already include the vacancy positions, thus no atoms had to be removed in that case (Fig. 13b).

As for the γ-P-model we could not perform frequency calculations for δ-FE due to the large size of the unit cell (160 atoms). δ-RH provides better results for the calculated lattice parameters (Table 11 and 12) with a relative error of 1.0% compared to δ-FE-Al_2O_3 (1.9%). The calculated band gaps of 6.6 eV and 7.2 eV, respectively, are direct transitions at the Γ-point. Regarding the energies per formula unit, δ-FE-Al_2O_3 is 9 kJ mol^{-1} more stable than δ-RH-Al_2O_3. However, this result must be taken with some care, since we used a simplified model for δ-RH and only analyzed one of a variety of possible vacancy arrangements. Moreover, the δ-RH-model is – unlike the δ-FE-model – based on crystallographic data of δ-Al_2O_3 and is considered as the more appropriate model in the end.

2.2.7 ι-Al_2O_3. The ι modification was already discovered in 1959 by Foster.[84] He found that X-ray diffraction patterns of a rapidly quenched melt of cryolite and aluminum oxide are very similar to those of a certain mullite compound. Even though there are later investigations of ι-Al_2O_3, *e.g.* by Korenko *et al.*,[85] there are no detailed experimental structural information yet. However, a theoretical study by Aryal *et al.*[86] revealed a possible structure model. It is based on the structure of a mullite compound ($Al_{2+2x}Si_{2-2x}O_{10-x}$, x = oxygen interstices per unit cell, space group *Pbam*, no. 55) with a very high Al : Si ratio ($Al_{2.826}Si_{0.174}O_{4.588}$). Starting from this compound the remaining silicon atoms were substituted by aluminum atoms and some oxygen atoms were removed to achieve the correct stoichiometry. One 2a position (0, 0, 0) is fully occupied and two 4h positions (x, y, 1/2) are partially occupied by aluminum atoms (58.7% and 41.3%). The oxygen atoms occupy a 4g Wyckoff position (x, y, 0) and a 4h position (x, y, 1/2) and a second 4h position by 25%. The unit cell suggested by Aryal *et al.* contains 240 atoms and is not used in this study because of the large computational costs. Instead we constructed a smaller cell (45 atoms) from a 1 × 1 × 3-supercell of Al-substituted mullite ($Al_{31}O_{36}$) and removed 13 aluminum and 9 oxygen atoms ($Al_{18}O_{27}$). First priority was to remove the aluminum atoms in a fashion that all Al–Al-distances are ≥3.0 Å. Afterwards selected oxygen atoms were removed with the aim that the remaining oxygen atoms stay in the vicinity of as many aluminum atoms as possible. We created three such models and chose the energetically lowest as the starting structure for geometry optimizations (Fig. 14).

As there are no experimental structure data available for ι-Al_2O_3, the theoretical model by Aryal *et al.* is used as a reference. With a relative deviation of the lattice constants of 9.3% our $Al_{18}O_{27}$ model significantly differs from the Aryal-model (Table 13). Schneider *et al.*[87] found that the lattice constant a of a mullite compound increases with increasing aluminum content. The parameter a of the starting compound $Al_{2.826}Si_{0.174}O_{4.588}$ is 7.739 Å, thus the observation Schneider *et al.* made applies to the Aryal-model with $a = 7.837$ Å, in contrast to our model with $a = 7.613$ Å. Taking this into account

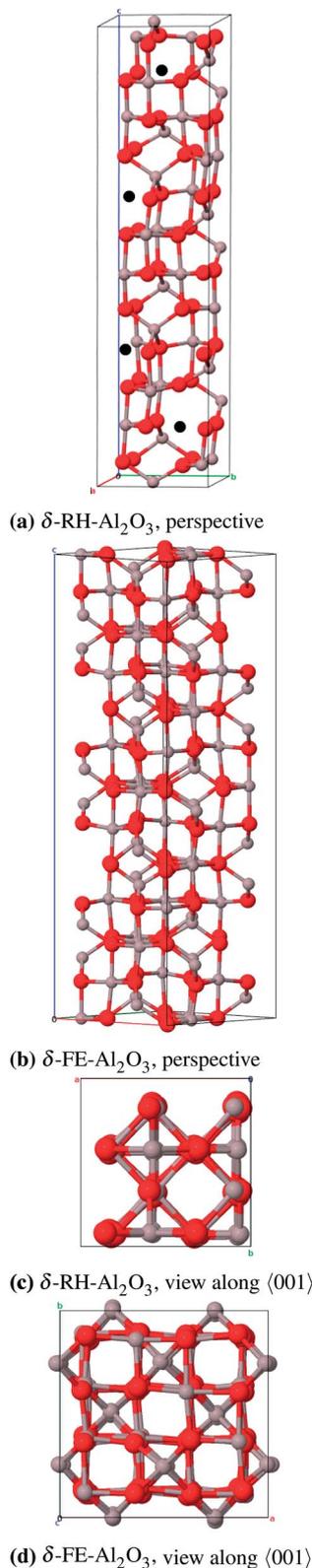**(a)** δ-RH-Al$_2$O$_3$, perspective

(b) δ-FE-Al$_2$O$_3$, perspective

(c) δ-RH-Al$_2$O$_3$, view along ⟨001⟩

(d) δ-FE-Al$_2$O$_3$, view along ⟨001⟩

Fig. 13   Primitive unit cell of δ-Al$_2$O$_3$ (vacancies: black).

Table 11 δ-FE-Al$_2$O$_3$ bulk properties, lattice constants a, c (Å), heat of atomization $\Delta_A H^0$ (kJ mol^{-1}) and fundamental band gap BG (eV)

	Calc.	Exp.
a	7.945	7.963[a]
c	23.790	23.398[a]
$\Delta_A H^0$	—	3072[b]
BG (direct)	7.2	—

[a] Ref. 79. [b] Ref. 50.

Table 12 δ-RH-Al$_2$O$_3$ bulk properties, lattice constants a, c (Å), heat of atomization $\Delta_A H^0$ (kJ mol^{-1}) and fundamental band gap BG (eV)

	Calc.	Exp.
a	5.633	5.599[a]
c	23.560	23.657[a]
$\Delta_A H^0$	2970	3072[b]
BG (direct)	6.6	—

[a] Ref. 78. [b] Ref. 50.

Table 13 ι-Al$_2$O$_3$ bulk properties, lattice constants a, b, c (Å), heat of atomization $\Delta_A H^0$ (kJ mol^{-1}) and fundamental band gap BG (eV)

	Calc.	Theor. comp-arative data[a]
a	7.613	7.837
b	7.213	7.583
c	3.045	2.996
$\Delta_A H^0$	2926	—
BG (indirect)	7.1	3.0

[a] Ref. 86.

indirect band gap of 7.1 eV. Taking into account the well-known self-interaction error of LDA which is reduced with hybrids, the PW1PW result is considered as more accurate. For a final clarification of the electronic structure it would be necessary to run a calculation of the Aryal-model with the PW1PW functional, which is, however, computationally demanding.

2.2.8 γ′-Al$_2$O$_3$. In 2004 Paglia *et al.*[5] observed during the calcination of boehmite that at 750 °C γ-Al$_2$O$_3$ did not turn into the δ- but into another modification which they named γ′. They determined its structure as a tripled unit cell of γ-Al$_2$O$_3$ with space group $P\bar{4}m2$ (no. 115), similar to Repelin and Husson's[78] structural description of δ-Al$_2$O$_3$. Nevertheless the structure of γ′-Al$_2$O$_3$ is way more complex as there appear octahedral as well as tetrahedral interstices and several positions are only partially occupied by aluminum atoms. Further increasing the calcination temperature resulted in a more ordered cation distribution so that the structure approaches that of δ-Al$_2$O$_3$ but still contains a few partially occupied positions.

In order to construct a supercell model with correct stoichiometry, 16 aluminum atoms had to be removed from the $P\bar{4}m2$-cell with fully occupied positions (Al$_{48}$O$_{48}$), resulting in a cell with 80 atoms (Al$_{32}$O$_{48}$). Unfortunately, all geometry

the Aryal-model is more appropriate for describing bulk properties of ι-Al$_2$O$_3$.

Aryal *et al.* calculated a direct band gap of 3 eV with an LDA functional. With the PW1PW hybrid functional we received an

13152 | *J. Mater. Chem. A*, 2014, **2**, 13143–13158

This journal is © The Royal Society of Chemistry 2014

(a) before relaxation
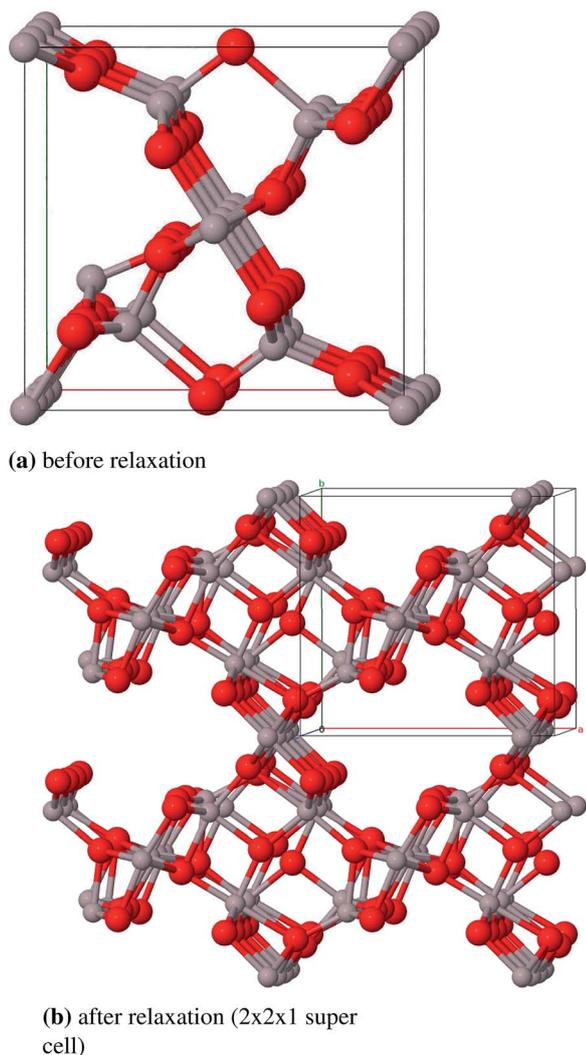
(b) after relaxation (2x2x1 super cell)

Fig. 14 Primitive unit cell of ι-Al_2O_3.

optimizations of this model led to extreme convergence problems with CRYSTAL-PW1PW. Therefore this structure was excluded from the energetic comparison.

2.2.9 κ'-Al_2O_3. Yamaguchi and Okumiya[88] investigated the κ'-Al_2O_3 phase with XRPD and suggested a structural model under the assumption that its structure is very similar to akdalaite (space group $P6_3mc$, no. 186). The oxygen atoms form a close-packed layered structure with the stacking sequence ABAC while the aluminum atoms are spread over several octahedral and tetrahedral interstices with most positions only partially occupied. The hexagonal unit cell proposed by Yamaguchi and Okumiya includes 16 oxygen and 32/3 aluminum atoms. Starting with a tripled Yamaguchi–Okumiya-cell with all positions fully occupied one gets a cell with the composition $Al_{84}O_{48}$ from which 52 aluminum atoms have to be removed. All of the models obtained in this way gave rise to severe SCF convergence problems, therefore, as for γ'-Al_2O_3, further investigation was not possible.

2.3 High-pressure Al_2O_3 polymorphs

For comparison with the Al_2O_3 polymorphs found at normal pressure we also studied metastable phases that can only be obtained under high pressure. With CRYSTAL it is possible to optimize the structure parameters of bulk unit cells with external hydrostatic pressure (EXTPRESS). This feature has been used in the following to calculate the structure and stability of high-pressure phases.

2.3.1 Rh_2O_3–Al_2O_3. The primitive, orthorhombic unit cell of Rh_2O_3–Al_2O_3 (space group $Pbcn$, no. 60) contains four formula units (Al_8O_{12}). All Al atoms occupy the Wyckoff position 8d (x, y, z) and are octahedrally surrounded by oxygen atoms located at positions 8d and 4c $(0, y, 1/4)$. By a Rietveld refinement at 113 GPa and 300 K Lin et al.[89] obtained structure data that were used as starting point for geometry optimization in this work (see Fig. 15).

The calculated lattice parameters (see Table 14) agree rather well with the experimental reference values. The deviations are less than 1.1%. The calculated direct band gap of 11.7 eV is very high compared to the other polymorphs.

2.3.2 $CaIrO_3$-Al_2O_3. The $CaIrO_3$ modification crystallizes in the orthorhombic crystal system as well (space group $Cmcm$, no. 63) and has a primitive unit cell containing ten atoms (Al_4O_6, conventional. cell: Al_8O_{12}). Half of the aluminum atoms are coordinated octahedrally (position 4c) and the other half tetrahedrally (position 4a) by oxygen atoms (position 4c and 8f).

Geometry optimization was performed taking atomic positions of $CaIrO_6$ from Sugahara et al.[90] and lattice constants for $CaIrO_3$–Al_2O_3 at room temperature and 150 GPa (XRPD) from
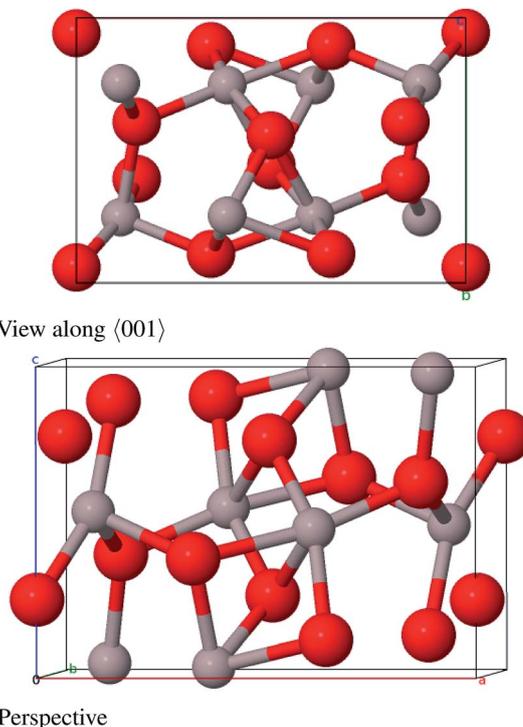
(a) View along $\langle 001 \rangle$

(b) Perspective

Fig. 15 Primitive unit cell of Rh_2O_3–Al_2O_3 at 113 GPa.

Table 14 Rh$_2$O$_3$–Al$_2$O$_3$ bulk properties, lattice constants a, b, c (Å) and fundamental band gap BG (eV) at 113 GPa

	Calc.	Exp.[a]
a	6.418	6.393
b	4.412	4.362
c	4.576	4.543
BG (direct)	11.7	—

[a] Ref. 89.

Table 15 CaIrO$_3$–Al$_2$O$_3$ bulk properties, lattice constants a, b, c (Å) and fundamental band gap BG (eV) at 150 GPa

	Calc.	Exp.[a]
a	2.441	2.431
b	8.017	7.925
c	6.078	6.053
BG (indirect)	10.8	—

[a] Ref. 34.

Ono and Oganov[34] as starting points. The optimized structure is shown in Fig. 16.

In Table 15 the calculated and measured lattice parameters are compared. There is good agreement between theory and experiment with deviations of the cell parameters being smaller than 1.2%. In this case the calculated band gap is indirect and has a value of 10.8 eV.

2.3.3 Stability of high pressure polymorphs. Fig. 17 and Table 16 show the relative stability of corundum and both high pressure modifications at various pressures. There is qualitative agreement between calculated and experimental results that α-Al$_2$O$_3$ is the most stable phase under atmospheric pressure, Rh$_2$O$_3$–Al$_2$O$_3$ around 113 GPa and CaIrO$_3$–Al$_2$O$_3$ around 150 GPa. The enthalpy–pressure curve in the shown area is only approximately linear. Making the linear approximation the

(a) View along $\langle 100 \rangle$

(b) Perspective

Fig. 16 Conventional unit cell of CaIrO$_3$–Al$_2$O$_3$ at 150 GPa.

transition to the Rh$_2$O$_3$ modification takes place around 88 GPa and is therefore within the experimentally found area of 80–100 GPa. The transition to the CaIrO$_3$ phase occures at about 132 GPa which is very close to the experimental value of about 130 GPa.

2.4 Relative stability

The relative stability of the Al$_2$O$_3$ phases and hydroxides is shown in Fig. 18 and Table 17. The hydroxides are thermodynamically more stable than all Al$_2$O$_3$ phases. Within the oxides gibbsite represents the most stable with an adjusted relative enthalpy of -189 kJ mol^{-1} followed by bayerite (-180 kJ mol^{-1}), boehmite (-85 kJ mol^{-1}) and akdalaite (-9 kJ mol^{-1}).
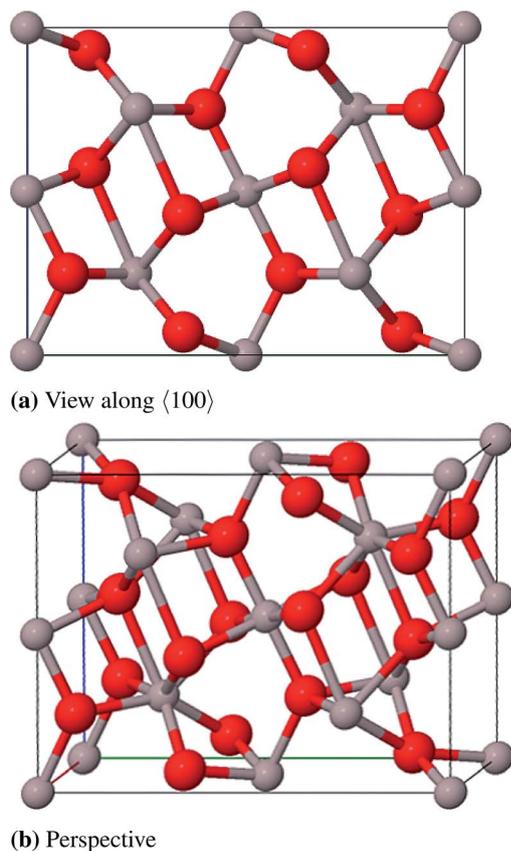
These findings are in agreement with previous studies[21,22] where gibbsite was found to be more stable by 7.7 kJ mol^{-1} than bayerite and boehmite is less stable than bayerite by 20.8 kJ mol^{-1} at B3LYP level.

κ-Al$_2$O$_3$ has a relative enthalpy $\Delta H(\alpha - \kappa)$ of 23 kJ mol^{-1}, close to the experimental value of 15 kJ mol^{-1} which was found in a calorimetric study by Yokokawa et al.[50] where also $\Delta H(\alpha - \gamma)$ and $\Delta H(\alpha - \delta)$ were determined.

Theoretical studies by Lee et al.[51] (plane-wave LDA) and Conesa et al.[82] (plane-wave GGA) obtained values of 20 kJ mol^{-1} and 11.5 kJ mol^{-1}, respectively, for $\Delta E(\alpha - \kappa)$. The latter work examined the impact of a dispersion correction (DFT-D) on the relative stability of several alumina phases. The uncorrected DFT calculations yielded 8.2 kJ mol^{-1} for $\Delta E(\alpha - \kappa)$ which means that the dispersion correcture led to a small change of 3.3 kJ mol^{-1} in this case. Thus we conclude that the neglect of dispersion corrections in the present study will not affect the main results.

With PW1PW the θ modification is less stable than κ-Al$_2$O$_3$ with a relative energy $\Delta E(\alpha - \theta)$ of 23 kJ mol^{-1} which agrees well with the LDA results of Lee et al. where the difference is 4 kJ mol^{-1}. At variance Conesa et al. determined the θ phase to be about 1 kJ mol^{-1} more stable than κ-Al$_2$O$_3$. There is no experimental reference value for $\Delta E(\alpha - \theta)$, but one can conclude from the calcination sequence of boehmite (Fig. 1) that the θ phase is probably even slightly more stable than δ-Al$_2$O$_3$ and thus more stable than κ-Al$_2$O$_3$.

The experimental values of $E(\alpha - \gamma)$, 22 kJ mol^{-1}, and $\Delta E(\alpha - \delta)$, 11 kJ mol^{-1}, are overestimated by 25 kJ mol^{-1} and 20 kJ mol^{-1}. From a solution calorimetry study of MgAl$_2$O$_4$·Al$_{8/3}$O$_4$ by Navrotsky et al.[91] a value for $\Delta H(\alpha - \gamma)$ of about 23 kJ mol^{-1} was derived which almost matches the value from Yokokawa

13154 | J. Mater. Chem. A, 2014, 2, 13143–13158

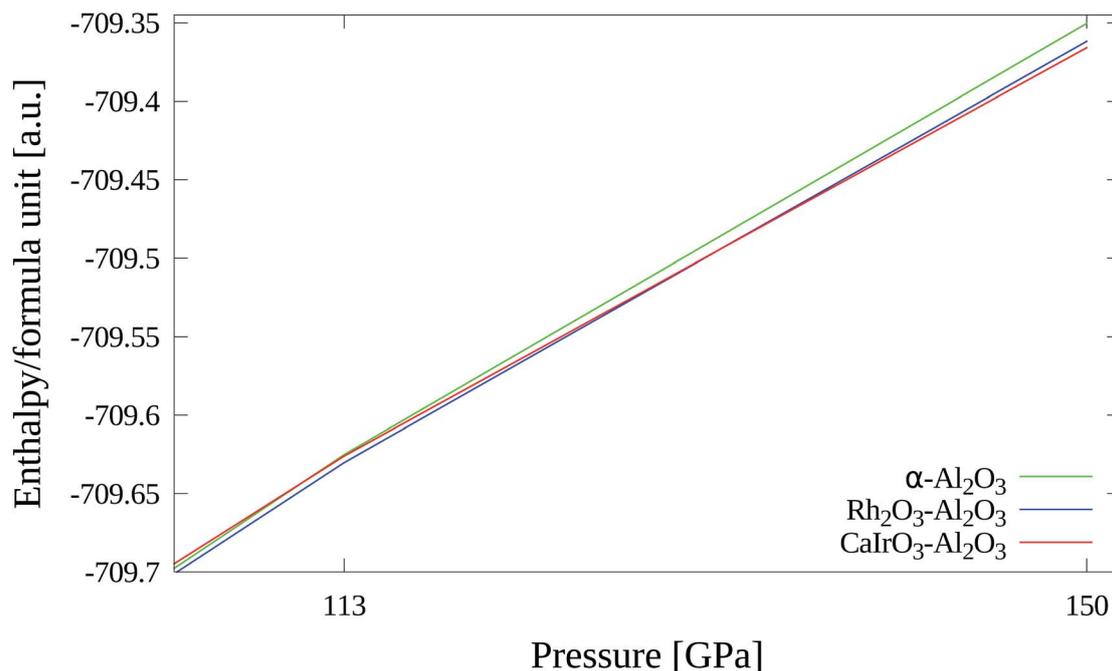This journal is © The Royal Society of Chemistry 2014

Fig. 17 Stability of high pressure phases from 113–150 GPa.

Table 16 Stability ΔH (kJ mol^{-1}) of high pressure phases at various pressures

	1013 hPa	113 GPa	150 GPa
α-Al$_2$O$_3$	0	+13	+41
Rh$_2$O$_3$–Al$_2$O$_3$	+44	0	+11
CaIrO$_3$–Al$_2$O$_3$	+131	+11	0

et al. As already mentioned energetically more favorable γ-cells may be derived from the Paglia-model if more defect configurations are considered. A possible explanation for the deviation of our results for δ-Al$_2$O$_3$ from experiment is the usage of a simplified model. According to our PW1PW calculations the η and ι phases are the least stable polymorphs with $\Delta E(\alpha - \eta) =$ 71 kJ mol^{-1} and $\Delta E(\alpha - \iota) = 74$ kJ mol^{-1}. There are no direct experimental or theoretical reference values for the relative stability of these two modifications. If the calcination process of bayerite (Fig. 1) is considered, η-Al$_2$O$_3$ is less stable than θ-Al$_2$O$_3$. Due to the similarity of η-Al$_2$O$_3$ and γ-Al$_2$O$_3$ it is plausible that there is no significant energetical difference between these two phases. As well as for the other self constructed models for the defective structures it can be assumed that energetically more favourable atomic configurations exist for that model.

3. Computational details

All quantum-chemical calculations were performed with a development version of the crystalline orbital program CRYSTAL.[92,93] Structure optimizations were performed employing the hybrid DFT functional PW1PW[94] which has been shown to provide good structural and thermochemical results for

oxides and other compounds.[94–96] The correlation functional is PW91 (ref. 97) while the exchange functional is a mixture of 20% Hartree–Fock (HF) and 80% PW91 exchange.

The performance of twelve DFT functionals in the study of crystal systems with the focus on aluminum hydroxides was investigated by Demichelis *et al.*[98] They found that recent GGA functionals reproduce the structure of orthosilicates quite well, but fail for the H-bonded layered Al hydroxides, where the inclusion of HF exchange in the hybrid functionals leads to a significant improvement.

The pob-DZVP basis sets recently developed by Peintinger *et al.*[99] were employed that have been parameterized for solid state systems. These basis sets were optimized in the same way as described here recently[100] and are available in the ESI.† The Monkhorst-Pack *k*-point-lattices have been converged for each system. The values of the shrinking factors are given in the ESI.†

4. Summary and conclusion

In this work we have investigated the structure, electronic structure and relative stability of alumina polymorphs. The PW1PW functional and the small pob-DZVP basis sets have delivered satisfactory results and have proven to be suitable for calculations of Al$_2$O$_3$ bulk properties for those modifications where sufficient experimental information about the atomic positions was available. To our knowledge this was the first time that models for the defective structures η- and δ-Al$_2$O$_3$ were constructed and quantum-chemically investigated. Exceptions are γ′-Al$_2$O$_3$ and κ′-Al$_2$O$_3$. Both represent defective structures with large unit cells and several partially occupied positions which makes the construction of a convergent cell very complex and time consuming. Besides the alumina phases four
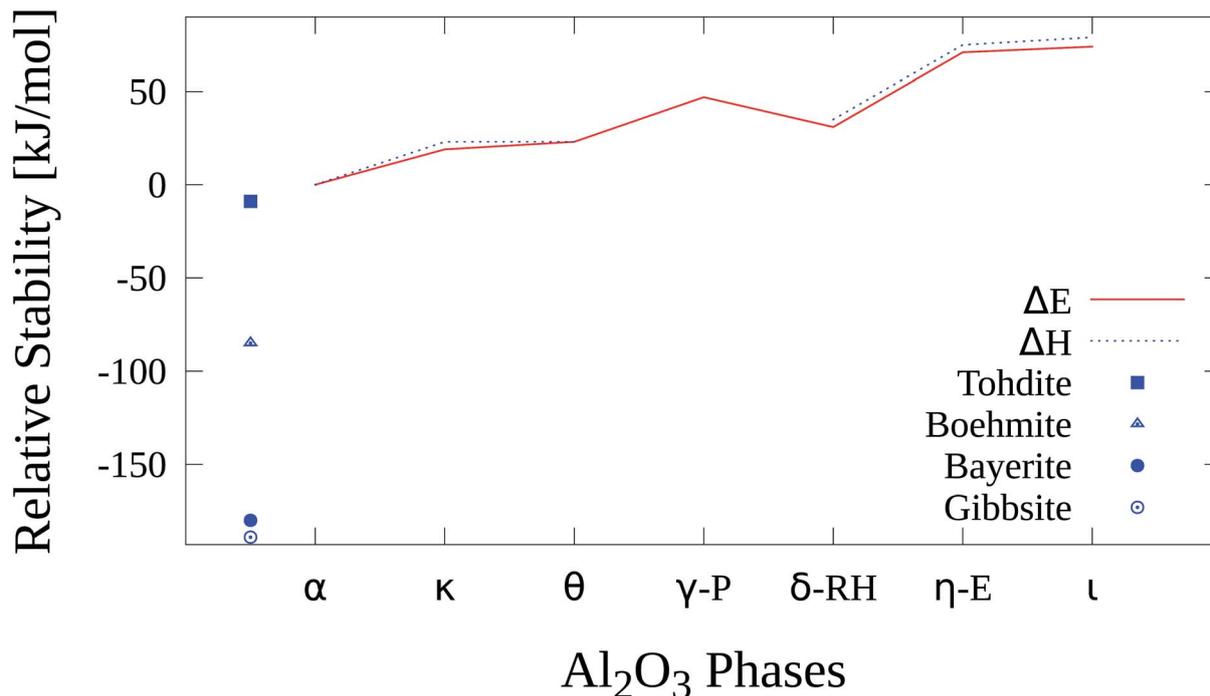
This journal is © The Royal Society of Chemistry 2014

J. Mater. Chem. A, 2014, **2**, 13143–13158 | **13155**

Fig. 18 Relative stability of Al_2O_3 phases and hydroxides.

Table 17 Relative stability ΔE^0, ΔH^0 (kJ mol^{-1}) of Al_2O_3 phases and hydroxides

	Gibbsite	Bayerite	Boehmite	Akdalaite	α-Al_2O_3	κ-Al_2O_3
ΔE^0	—	—	—	—	0	+19
ΔH^0	−189	−180	−85	−9	0	+23

	θ-Al_2O_3	γ-P-Al_2O_3	δ-RH-Al_2O_3	η-E-Al_2O_3	ι-Al_2O_3
ΔE^0	+23	+47	+31	+71	+74
ΔH^0	+23	—	+35	+75	+79

aluminum hydroxides were successfully investigated and added to the relative stability comparison. We received reasonable results for the lattice constants. A dispersion correction[101] is expected to further improve the agreement with experiment for the layer structures. Due to the computational expense frequency calculations for the thermodynamic functions were not feasible for all systems, but it was concluded that the relative energies only slightly deviate from the relative enthalpies because of cancellation effects. The following energetic order was obtained: gibbsite < bayerite < boehmite < akdalaite < α-Al_2O_3 < κ-Al_2O_3 < θ-Al_2O_3 < δ-Al_2O_3 < γ-Al_2O_3 < η-Al_2O_3 < ι-Al_2O_3. This agrees with earlier studies except for δ-Al_2O_3 which was found to be more stable than κ-Al_2O_3. A possible cause for this discrepancy is the simplified model for δ-Al_2O_3 besides inaccuracies of the functional and basis set. For a further improvement of the accuracy a gcp-correction[102] is desirable which takes basis set errors into account in structure optimizations. The implementation of these corrections into CRYSTAL

is currently in progress. Both high-pressure phases were part of this study as well. The calculated results agree with the experiments that the Rh_2O_3 modification is the most stable phase at 113 GPa and the $CaIrO_3$ modification is the ground state at 150 GPa. Moreover the transition pressures is well reproduced by the calculations. So α-Al_2O_3 transforms to the Rh_2O_3 phase at about 88 GPa (exp. 80–100 GPa) which is transformed to the $CaIrO_3$ phase at about 132 GPa (exp. 130 GPa).

Acknowledgements

References

1   J. H. Eggert, K. A. Goettel and I. F. Silvera, *Phys. Rev. B: Condens. Matter Mater. Phys.*, 1989, **40**, 5724.

2   R. G. McQueen and D. G. Isaak, *JGR, J. Geophys. Res.*, 1990, **95**, 21753–21765.

3   S. Vuorinen and J. Skogsmo, *Thin Solid Films*, 1990, **193**, 536–546.

4   C. G. Chatfield, J. N. Lindstrom, M. E. K. Sjostrand and I. K. M. Collin, *CVD of Al₂O₃ layers on cutting inserts*, 1996, US Patent 5,543,176.

5 G. Paglia, C. E. Buckley, A. L. Rohl, R. D. Hart, K. Winter, A. J. Studer, B. A. Hunter and J. V. Hanna, *Chem. Mater.*, 2004, **16**, 220–236.

6 M. Minnermann, B. Neumann, V. Zielasek and M. Baumer, *Catal. Sci. Technol.*, 2013, **3**, 3256–3267.

7 S.-H. Cai, S. N. Rashkeev, S. T. Pantelides and K. Sohlberg, *Phys. Rev. B: Condens. Matter Mater. Phys.*, 2003, **67**, 224104.

8 R. McPherson, *J. Mater. Sci.*, 1980, **15**, 3141–3149.

9 J. K. Bristow, D. Tiana, S. C. Parker and A. Walsh, *J. Mater. Chem. A*, 2014, **2**, 6198–6208.

10 A. B. Dichiara, J. Yuan, S. Yao, A. Sylvestre, L. Zimmer and J. Bai, *J. Mater. Chem. A*, 2014, **2**, 7980–7987.

11 Z. Xie, T. Li, N. L. Rosi and M. A. Carreon, *J. Mater. Chem. A*, 2014, **2**, 1239–1241.

12 G. J. B. Voss, E. A. Chavez Panduro, A. Midttveit, J. B. Floystad, K. Hoydalsvik, A. Gibaud, D. W. Breiby and M. Ronning, *J. Mater. Chem. A*, 2014, **2**, 9727–9735.

13 Y.-S. Lee, A. S. K. Kaliyappan, G. Kim and K. S. Nahm, *RSC Adv.*, 2014, **4**, 23107–23115.

14 R. Musat, G. Vigneron, D. Garzella, S. LeCaer, J. F. Hergott, J. P. Renault and S. Pommeret, *Chem. Commun.*, 2010, **46**, 2394–2396.

15 M. W. Jung, W. Song, W. J. Choi, D. S. Jung, Y. J. Chung, S. Myung, S. S. Lee, J. Lim, C.-Y. Park, J.-O. Lee and K.-S. An, *J. Mater. Chem. C*, 2014, **2**, 4759–4763.

16 R. Demichelis, Y. Noel, C. Zicovich-Wilson, C. Roetti, L. Valenzano and R. Dovesi, *J. Phys.: Conf. Ser.*, 2008, 012013.

17 R. Demichelis, B. Civalleri, Y. Noel, A. Meyer and R. Dovesi, *Chem. Phys. Lett.*, 2008, **465**, 220–225.

18 Y. Noel, R. Demichelis, F. Pascale, P. Ugliengo, R. Orlando and R. Dovesi, *Phys. Chem. Miner.*, 2009, **36**, 47–59.

19 R. Demichelis, Y. Noel, B. Civalleri, C. Roetti, M. Ferrero and R. Dovesi, *J. Phys. Chem. B*, 2007, **111**, 9337–9346.

20 R. Demichelis, M. Catti and R. Dovesi, *J. Phys. Chem. C*, 2009, **113**, 6785–6791.

21 R. Demichelis, Y. Noöl, P. Ugliengo, C. M. Zicovich-Wilson and R. Dovesi, *J. Phys. Chem. C*, 2011, **115**, 13107–13134.

22 S. Casassa and R. Demichelis, *J. Phys. Chem. C*, 2012, **116**, 13313–13321.

23 I. Levin and D. Brandon, *J. Am. Ceram. Soc.*, 1998, **81**, 1995–2012.

24 R. Poisson, J. P. Brunelle, P. Nortier and A. B. Stiles, *Catalyst Supports and Supported Catalysts. Theoretical and Applied Concepts*, ed. A.B. Stiles, Butterworths, Boston, 1987.

25 D. Ksenofontov and Y. K. Kabalov, *Inorg. Mater.*, 2012, **48**, 142–144.

26 T. Ishigaki, Y. Bando, Y. Moriyoshi and M. Boulos, *J. Mater. Sci.*, 1993, **28**, 4223–4228.

27 H. C. Stumpf, A. S. Russell, J. W. Newsome and C. M. Tucker, *Ind. Eng. Chem.*, 1950, **42**, 1398–1403.

28 G. W. Brindley and J. O. Choe, *Am. Mineral.*, 1961, **46**, 771–785.

29 M. U. Devi, *Ceram. Int.*, 2004, **30**, 555–565.

30 I. Levin, L. A. Bendersky, D. G. Brandon and M. Rühle, *Acta Mater.*, 1997, **45**, 3659–3669.

31 I. Levin, T. Gemming and D. G. Brandon, *Phys. Status Solidi A*, 1998, **166**, 197–218.

32 I. Levin and D. G. Brandon, *Philos. Mag. Lett.*, 1998, **77**, 117–124.

33 A. R. Oganov and S. Ono, *Proc. Natl. Acad. Sci. U. S. A.*, 2005, **102**, 10828–10831.

34 S. Ono, A. R. Oganov, T. Koyama and H. Shimizu, *Earth Planet. Sci. Lett.*, 2006, **246**, 326–335.

35 J. Moellmann, S. Ehrlich, R. Tonner and S. Grimme, *J. Phys.: Condens. Matter*, 2012, **24**, 424206.

36 A. N. Christensen, M. S. Lehmann and P. Convert, *Acta Chem. Scand.*, 1982, **36**, 303–308.

37 H. Saalfeld and M. Wedde, *Z. Kristallogr.*, 1974, **139**, 129–135.

38 F. Zigan, W. Joswig and N. Burger, *Z. Kristallogr.*, 1978, **148**, 255–273.

39 G. Yamaguchi, M. Okumiya and S. Ono, *Bull. Chem. Soc. Jpn.*, 1969, **42**, 2247–2249.

40 M. Digne, P. Sautet, P. Raybaud, H. Toulhoat and E. Artacho, *J. Phys. Chem. B*, 2002, **106**, 5155–5162.

41 D. W. Bennett, *Understanding Single-Crystal X-Ray Crystallography*, Wiley-VCH, Weinheim, 2010, pp. 12–34.

42 L. Lutterotti and P. Scardi, *J. Appl. Crystallogr.*, 1990, **23**, 246–252.

43 *NIST Chemistry WebBook, NIST Standard Reference Database Number 69*, ed. P. Linstrom and W. Mallard, National Institute of Standards and Technology, 2009.

44 J. Olivier and R. Poirier, *Surf. Sci.*, 1981, **105**, 347–356.

45 W. Y. Ching and Y.-N. Xu, *J. Am. Ceram. Soc.*, 1994, **77**, 404–411.

46 J. Skogsmo, P. Liu, C. Chatfield and H. Norden, *12 th International Plansee Seminar 89*, 1989, pp. 129–142.

47 P. Liu and J. Skogsmo, *Acta Crystallogr., Sect. B: Struct. Sci.*, 1991, **47**, 425–433.

48 H.-L. Gross and W. Mader, *Chem. Commun.*, 1997, 55–56.

49 B. Ollivier, R. Retoux, P. Lacorre, D. Massiot and G. Férey, *J. Mater. Chem.*, 1997, **7**, 1049–1056.

50 T. Yokokawa and O. Kleppa, *J. Phys. Chem.*, 1964, **68**, 3246–3249.

51 C.-K. Lee, E. Cho, H.-S. Lee, K. S. Seol and S. Han, *Phys. Rev. B: Condens. Matter Mater. Phys.*, 2007, **76**, 245110.

52 E. Husson and Y. Repelin, *Eur. J. Solid State Inorg. Chem.*, 1996, **33**, 1223–1231.

53 E. Menendez-Proupin and G. Gutierrez, *Phys. Rev. B: Condens. Matter Mater. Phys.*, 2005, **72**, 035116.

54 W.-Y. Ching, L. Ouyang, P. Rulis and H. Yao, *Phys. Rev. B: Condens. Matter Mater. Phys.*, 2008, **78**, 014106.

55 T. Hahn, *International tables for crystallography. Volume A, Space-group symmetry*, Kluwer Academic Publishers, 1995.

56 B. C. Lippens and J. H. De Boer, *Acta Crystallogr.*, 1964, **17**, 1312–1321.

57 G. Paglia, C. E. Buckley, T. J. Udovic, A. L. Rohl, F. Jones, C. F. Maitland and J. Connolly, *Chem. Mater.*, 2004, **16**, 1914–1923.

58 C. Wolverton and K. Hass, *Phys. Rev. B: Condens. Matter Mater. Phys.*, 2000, **63**, 024102.

This journal is © The Royal Society of Chemistry 2014

J. Mater. Chem. A, 2014, **2**, 13143–13158 | **13157**

59 G. N. Kryukova, D. O. Klenov, A. S. Ivanova and S. V. Tsybulya, *J. Eur. Ceram. Soc.*, 2000, **20**, 1187–1189.

60 D. Y. Li, B. H. O'Conner, G. I. D. Roach and J. B. Cornell, *XVth Congress of the International Union of Crystallography (Bordeaux)*, 1990.

61 V. Jayaram and C. G. Levi, *Acta Metall. Mater.*, 1989, **37**, 569–578.

62 H. Saalfeld and B. Mehrotra, *Ber. Dtsch. Keram. Ges*, 1965, **42**, 161–166.

63 J. Wang, X. Bokhimi, A. Morales, O. Novaro, T. Lopez and R. Gomez, *J. Phys. Chem. B*, 1999, **103**, 299–303.

64 M.-H. Lee, C.-F. Cheng, V. Heine and J. Klinowski, *Chem. Phys. Lett.*, 1997, **265**, 673–676.

65 S.-D. Mo, Y.-N. Xu and W.-Y. Ching, *J. Am. Ceram. Soc.*, 1997, **80**, 1193–1197.

66 F. H. Streitz and J. W. Mintmire, *Phys. Rev. B: Condens. Matter Mater. Phys.*, 1999, **60**, 773.

67 G. Gutiérrez, A. Taga and B. Johansson, *Phys. Rev. B: Condens. Matter Mater. Phys.*, 2001, **65**, 012101.

68 R.-S. Zhou and R. L. Snyder, *Acta Crystallogr., Sect. B: Struct. Sci.*, 1991, **47**, 617–630.

69 G. Paglia, C. E. Buckley, A. L. Rohl, B. A. Hunter, R. D. Hart, J. V. Hanna and L. T. Byrne, *Phys. Rev. B: Condens. Matter Mater. Phys.*, 2003, **68**, 144110.

70 G. Paglia, A. L. Rohl, C. E. Buckley and J. D. Gale, *Phys. Rev. B: Condens. Matter Mater. Phys.*, 2005, **71**, 224115.

71 E. Menéndez-Proupin and G. Gutiérrez, *Phys. Rev. B: Condens. Matter Mater. Phys.*, 2005, **72**, 035116.

72 H. P. Pinto, R. Nieminen and S. D. Elliott, *Phys. Rev. B: Condens. Matter Mater. Phys.*, 2004, **70**, 125402.

73 A. R. Ferreira, M. J. Martins, E. Konstantinova, R. B. Capaz, W. F. Souza, S. S. X. Chiaro and A. A. Leitão, *J. Solid State Chem.*, 2011, **184**, 1105–1111.

74 K. Shirasuka, H. Yanagida and G. Yamaguchi, *J. Ceram. Assoc.*, 1976, **84**, 610–613.

75 F. Ernst, P. Pirouz and A. Heuer, *Philos. Mag. A*, 1991, **63**, 259–277.

76 S. J. Wilson, *Mineral. Mag.*, 1979, **43**, 301–306.

77 S. J. Wilson, *J. Solid State Chem.*, 1979, **30**, 247–255.

78 Y. Repelin and E. Husson, *Mater. Res. Bull.*, 1990, **25**, 611–621.

79 S. V. Tsybulya and G. N. Kryukova, *Powder Diffr.*, 2003, **18**, 309–311.

80 Y. G. Wang, P. M. Bronsveld, J. T. M. DeHosson, B. Djuričić, D. McGarry and S. Pickering, *J. Am. Ceram. Soc.*, 1998, **81**, 1655–1660.

81 J.-E. Jørgensen, L. Mosegaard, L. E. Thomsen, T. R. Jensen and J. C. Hanson, *J. Solid State Chem.*, 2007, **180**, 180–185.

82 J. C. Conesa, *J. Phys. Chem. B*, 2010, **114**, 22718–22726.

83 C. Pecharroman, I. Sobrados, J. E. Iglesias, T. Gonzalez-Carreno and J. Sanz, *J. Phys. Chem. B*, 1999, **103**, 6160–6170.

84 P. A. Foster, *J. Electrochem. Soc.*, 1959, **106**, 971–975.

85 M. Korenko, M. Kuchárik and D. Janičkovi&ccaron, *Chem. Pap.*, 2008, **62**, 219–222.

86 S. Aryal, P. Rulis, L. Ouyang and W. Y. Ching, *Phys. Rev. B: Condens. Matter Mater. Phys.*, 2011, **84**, 174123.

87 H. Schneider, J. Schreuer and B. Hildmann, *J. Eur. Ceram. Soc.*, 2008, **28**, 329–344.

88 M. Okumiya and G. Yamaguchi, *Bull. Chem. Soc. Jpn.*, 1971, **44**, 1567–1570.

89 J.-F. Lin, O. Degtyareva, C. T. Prewitt, P. Dera, N. Sata, E. Gregoryanz, H.-k. Mao and R. J. Hemley, *Nat. Mater.*, 2004, **3**, 389–393.

90 M. Sugahara, A. Yoshiasa, A. Yoneda, T. Hashimoto, S. Sakai, M. Okube, A. Nakatsuka and O. Ohtaka, *Am. Mineral.*, 2008, **93**, 1148–1152.

91 A. Navrotsky, B. A. Wechsler, K. Geisinger and F. Seifert, *J. Am. Ceram. Soc.*, 1986, **69**, 418–422.

92 R. Dovesi, V. R. Saunders, C. Roetti, R. Orlando, C. M. Zicovich-Wilson, F. Pascale, B. Civalleri, K. Doll, N. M. Harrison, I. J. Bush, P. D'Arco and M. Llunell, *CRYSTAL09 User's Manual*, University of Torino, Torino, 2009.

93 R. Dovesi, V. R. Saunders, C. Roetti, R. Orlando, C. M. Zicovich-Wilson, F. Pascale, B. Civalleri, K. Doll, N. M. Harrison, I. J. Bush, P. D'Arco, M. Llunell, M. Causà and Y. Noël, CRYSTAL14 User's Manual, University of Torino, Torino, 2014.

94 T. Bredow and A. R. Gerson, *Phys. Rev. B: Condens. Matter Mater. Phys.*, 2000, **61**, 5194.

95 T. Bredow, *Phys. Rev. B: Condens. Matter Mater. Phys.*, 2007, **75**, 144102.

96 M. M. Islam, T. Bredow and C. Minot, *J. Phys. Chem. B*, 2006, **110**, 9413–9420.

97 J. P. Perdew and Y. Wang, *Phys. Rev. B: Condens. Matter Mater. Phys.*, 1992, **45**, 13244–13249.

98 R. Demichelis, B. Civalleri, P. D'Arco and R. Dovesi, *Int. J. Quantum Chem.*, 2010, **110**, 2260–2273.

99 M. F. Peintinger, D. V. Oliveira and T. Bredow, 2014, unpublished.

100 M. F. Peintinger, D. V. Oliveira and T. Bredow, *J. Comput. Chem.*, 2012, **34**, 451–459.

101 W. Reckien, F. Janetzko, M. F. Peintinger and T. Bredow, *J. Comput. Chem.*, 2012, **33**, 2023–2031.

102 J. G. Brandenburg, M. Alessio, B. Civalleri, M. F. Peintinger, T. Bredow and S. Grimme, *J. Phys. Chem. A*, 2013, **117**, 9282–9292.

13158 | *J. Mater. Chem. A*, 2014, **2**, 13143–13158

This journal is © The Royal Society of Chemistry 2014